PNAS RESEARCH ARTICLE | NEUROSCIENCE

Neuronal mechanism of a BK channelopathy in absence epilepsy and dyskinesia

Ping Dong[a], Yang Zhang[a], Arsen S. Hunanyan[b], Mohamad A. Mikati[b,c], Jianmin Cui[d], and Huanghe Yang[a,c,1]

Edited by Hee-Sup Shin, Institute for Basic Science, Daejeon, South Korea; received January 13, 2022; accepted February 2, 2022

A growing number of gain-of-function (GOF) BK channelopathies have been identified in patients with epilepsy and movement disorders. Nevertheless, the underlying pathophysiology and corresponding therapeutics remain obscure. Here, we utilized a knock-in mouse model carrying human BK-D434G channelopathy to investigate the neuronal mechanism of BK GOF in the pathogenesis of epilepsy and dyskinesia. The BK-D434G mice manifest the clinical features of absence epilepsy and exhibit severe motor deficits and dyskinesia-like behaviors. The cortical pyramidal neurons and cerebellar Purkinje cells from the BK-D434G mice show hyperexcitability, which likely contributes to the pathogenesis of absence seizures and paroxysmal dyskinesia. A BK channel blocker, paxilline, potently suppresses BK-D434G–induced hyperexcitability and effectively mitigates absence seizures and locomotor deficits in mice. Our study thus uncovered a neuronal mechanism of BK GOF in absence epilepsy and dyskinesia. Our findings also suggest that BK inhibition is a promising therapeutic strategy for mitigating BK GOF-induced neurological disorders.

BK channel | channelopathy | epilepsy | dyskinesia | absence seizure

KCNMA1 encodes the pore-forming α subunit of the Ca^{2+}- and voltage-activated large-conductance BK-type potassium channels, which are widely expressed in the brain with high expression levels in the cortex, cerebellar Purkinje cells (PCs), thalamus, hippocampus, basal ganglia, habenula, and olfactory bulb (1–4). Owing to its large single-channel conductance, its dual sensitivity to both voltage and intracellular Ca^{2+}, and its spatial proximity to voltage-gated Ca^{2+} channels (VGCCs) (4–9) (Fig. 1*A*), BK channels play pivotal roles in shaping action potential (AP) repolarization, giving rise to fast afterhyperpolarization (fAHP), controlling dendritic Ca^{2+} spikes and influencing synaptic transmission (1, 2, 10–12). Consistent with its importance in the nervous system, dysfunction of BK channels has been implicated in the pathophysiology of various neurological disorders including epilepsy (12–16), movement disorders (13, 15, 17–23), and neurodevelopmental and cognitive disorders such as intellectual delay (15, 16, 18, 21, 24), autism spectrum disorder (14, 17, 21, 25), fragile X syndrome (26), and Angelman syndrome (27). How BK channels are involved in such a diverse spectrum of neurological disorders (28–31), however, remains largely elusive and demands in-depth studies.

KCNMA1 variants identified from human genetic analysis provide unique opportunities to understand the neurological functions of BK channels (28, 30). The first *KCNMA1*-linked potassium channelopathy, D434G, was found in a large family of patients with generalized epilepsy and/or paroxysmal nonkinesigenic dyskinesia (PNKD), and the pedigree analysis indicated that *D434G* mutation is inherited as autosomal-dominant (13). Of the 16 BK-D434G patients, 9 individuals had absence epilepsy, which is characterized by sudden, brief lapses of consciousness accompanied by behavioral arrest and distinctive bilaterally synchronous spike-and-wave discharges (SWDs) at 3 to 4 Hz (32) (Table 1); 12 BK-D434G patients developed PNKD, which is an episodic movement disorder characterized as involuntary dystonic or choreiform movements with intact consciousness (13). Interestingly, five BK-D434G patients were affected by both absence epilepsy and PNKD. Subsequent biophysical characterizations demonstrated that BK-D434G is a gain-of-function (GOF) mutation with enhanced Ca^{2+} sensitivity (13, 23, 33–35). It is intriguing why a GOF potassium channel mutation is associated with epilepsy and dyskinesia, which is characterized by hyperexcitability and hypersynchronization in nature. A growing number of human *KCNMA1* variants have been identified over the past several years (28, 30). However, it is unknown 1) whether the *KCNMA1* variants cause the associated neurological disorders, 2) how the *KCNMA1* variants affect neuronal activities at cellular level, and 3) whether targeting the mutant BK channels is effective to mitigate the associated neurological symptoms.

To address these questions, we characterized a knock-in mouse model carrying the BK-D434G mutation. We found that the BK-D434G mice align with the clinical

Significance

BK channelopathy has been increasingly implicated in diverse neurological disorders, including epilepsy and movement, cognitive, and neurodevelopmental disorders. However, precision medicine to treat BK channelopathy is lacking. We characterized a mouse model carrying a gain-of-function BK channelopathy D434G from a large family of patients with absence epilepsy and paroxysmal dyskinesia. The BK-D434G mice manifest the clinical features of absence seizures and exhibit severe locomotor defects including involuntary dyskinesia-like behavior. Pharmacological inhibition of BK channels suppresses neuronal hyperactivity and mitigates absence seizure and the locomotor defects. The BK-D434G mice thus serve as a model to understand the pathogenic mechanisms of absence epilepsy and dyskinesia. Our study also suggests that BK inhibition is a promising strategy for treating BK gain-of-function channelopathy.

Author contributions: P.D., J.C., and H.Y. designed research; P.D. and Y.Z. performed research; A.S.H., M.A.M., J.C., and H.Y. contributed new reagents/analytic tools; P.D., Y.Z., and H.Y. analyzed data; H.Y. provided funding; and P.D., M.A.M., J.C., and H.Y. wrote the paper.

The authors declare no competing interest.

This article is a PNAS Direct Submission.

[1]To whom correspondence may be addressed. Email: huanghe.yang@duke.edu.

This article contains supporting information online at http://www.pnas.org/lookup/suppl/doi:10.1073/pnas.2200140119/-/DCSupplemental.

Published March 14, 2022.

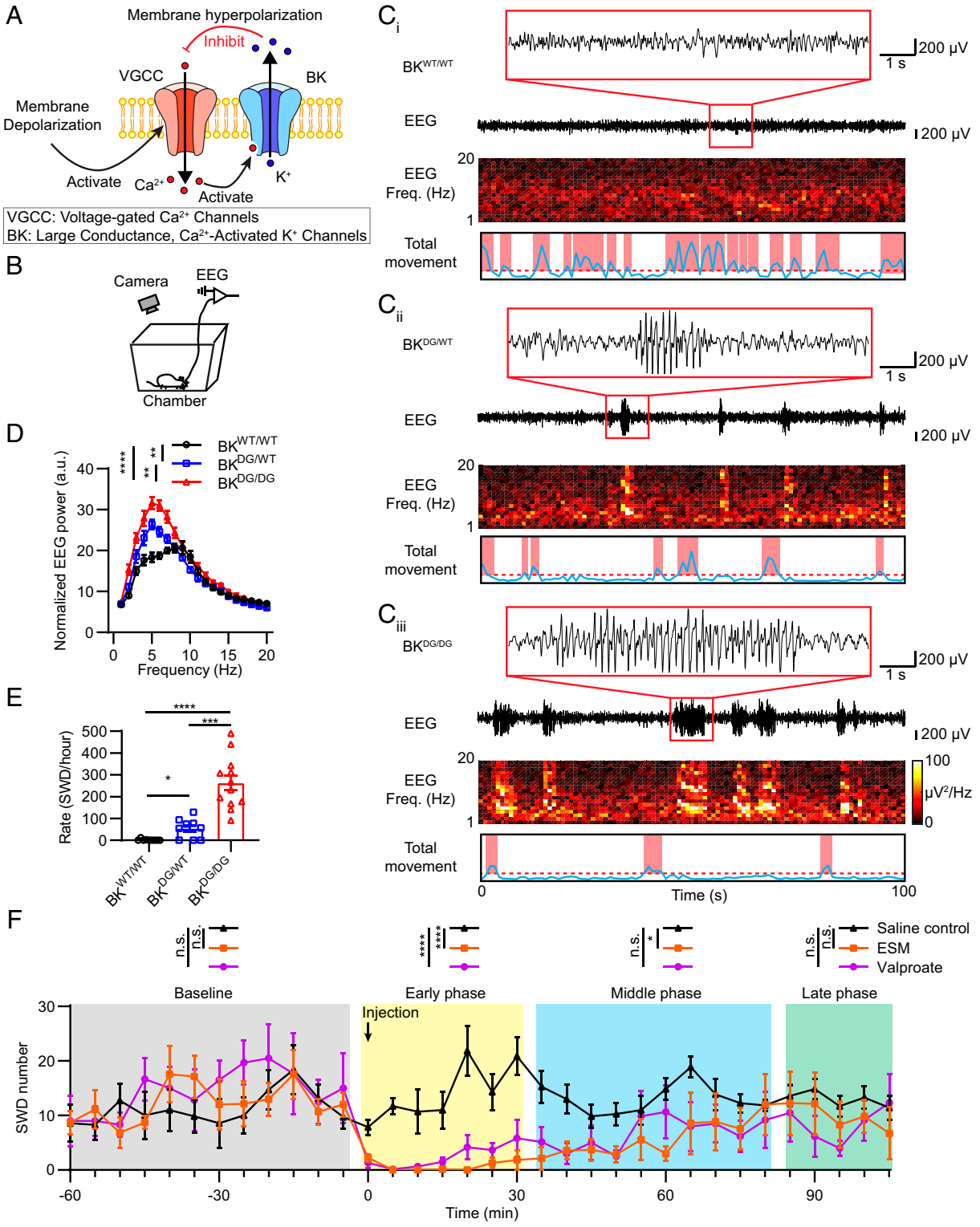

Fig. 1. BK-D434G knock-in mice have spontaneous absence seizures and responded to first-line antiabsence medicines. (*A*) Ca^{2+}- and voltage-activated BK channels control the opening of voltage-gated Ca^{2+} channels (VGCCs or Ca_Vs) through a negative-feedback mechanism. (*B*) Schematic of the simultaneous video-EEG recordings of freely moving mice. (*C*) $BK^{DG/WT}$ (*C_{ii}*) and $BK^{DG/DG}$ (*C_{iii}*) but not $BK^{WT/WT}$ mice (*C_i*) had spontaneous SWDs and frequent behavior arrest. (*Top*) Raw EEG traces. Red rectangles show the corresponding EEG traces on an expanded time scale. (*Middle*) Corresponding spectrograms of the EEG traces. (*Bottom*) Video-based analysis of the total movement. The behavior status is classified as motion state (red boxes) or immobile state (white boxes). See *Methods* for details. (*D*) Summary of power spectral density of EEG recorded from $BK^{WT/WT}$ (n = 9), $BK^{DG/WT}$ (n = 9), and $BK^{DG/DG}$ (n = 12) mice. Normalization was performed by averaging the power to the total recording time. Two-way ANOVA, $F_{(2,27)} = 9.683$, $P = 0.0007$. (*E*) Summary of the number of spontaneous SWDs per hour for from $BK^{WT/WT}$ (n = 9), $BK^{DG/WT}$ (n = 9), and $BK^{DG/DG}$ (n = 12) mice. One-way ANOVA test, $F_{(2,27)} = 11.57$, $P = 0.0002$. (*F*) Time course of the drug effects of ESM (orange), valproate (purple), and saline control (black) on the spontaneous SWDs of the $BK^{DG/DG}$ mice (bin size = 5 min). The drug effects were empirically divided into four different phases: baseline phase, 60 min prior to injection [gray box, two-way repeated-measures ANOVA, $F_{(2,17)} = 1.176$, $P = 0.3324$]; early phase, 30 min postinjection [yellow box, two-way repeated-measures ANOVA, $F_{(2,17)} = 78.61$, $P < 0.0001$]; middle phase, from 35 to 80 min postinjection [blue box, two-way repeated-measures ANOVA, $F_{(2,17)} = 3.906$, $P = 0.0402$]; and late phase, from 85 to 105 min postinjection [green box, two-way repeated-measures ANOVA, $F_{(2,17)} = 0.5274$, $P = 0.5274$]. n = 7 mice per group for saline control and ESM; n = 6 mice for valproate administration. In all plots and statistical tests, summary graphs show mean ± SEM; *$P < 0.05$, **$P < 0.01$, ***$P < 0.01$, ****$P < 0.0001$. n.s., not statistically significant.

Table 1. Comparison of absence seizures in human patients and rodent models

	Typical human absence seizure	BK-D434G proband	BK-D434G mouse	Tottering mouse	WAG/Rij rat
EEG					
Onset age	3 y	<6 mo	<4 wk	3 wk	>75 d
Generalized synchronous SWD	+	+	+	+	+
SWD frequency, Hz	3–4	3–4	3–8	6–7	7–11
SWD duration, s	4–20	N/A	0.5–10	0.3–10	1–45
Ictal behavior					
Staring: myoclonus	+	+	+	+	+
Move during SWD	–	–	–	–	–
Pharmacology					
ESM	+	N/A	+	+	+
Valproate	+	+	+	+	+
Refs.	39, 54, 57, 73	13	Current study	74, 75	76, 77

N/A: not applicable or not available.

manifestations of the patients. The mutant mice had frequent spontaneous absence seizures, which can be controlled by first-line antiabsence medications. The mutant mice also exhibit dyskinesia-like behaviors, which are exacerbated by stress, alcohol, and a muscarinic acetylcholine receptor agonist. In addition, the animals show motor defects in a battery of locomotor tests. In vitro brain slice recordings revealed that the hyperexcitability of the cortical pyramidal neurons and PCs from the BK-D434G mice likely contributes to absence seizures and the movement deficiency. The effectiveness of paxilline (PAX), a BK channel-specific blocker, on suppressing BK-D434G–induced absence seizures and locomotor defects in the BK-D434G mice highlights a promising therapeutic strategy to mitigate BK GOF-induced neurological disorders.

Results

BK-D434G Knock-In Mice Manifest the Clinical Features of Absence Epilepsy. A knock-in mouse line carrying BK-D434G mutation was generated by homologous recombination (*SI Appendix*, Fig. S1*A* and *Methods*). The resulting animals were confirmed by both genotyping PCR (*SI Appendix*, Fig. S1*B*) and genomic sequencing (*SI Appendix*, Fig. S1*C*). The heterozygous BK-D434G mutation ($BK^{DG/WT}$) mice, which recapitulate the patient genotype, were viable and survived into adulthood. On the other hand, only 17.3% of the offspring were homozygous $BK^{DG/DG}$ under the $BK^{DG/WT} \times BK^{DG/WT}$ breeding scheme, which was significantly less than the expected 25% Mendelian inheritance ($P < 0.05$, $\chi^2 = 6.495$; *SI Appendix*, Fig. S1*D*). However, Kaplan–Meier analysis of postnatal survival curves did not show evidence of postnatal lethality (data not shown), suggesting that BK-D434G mutation homozygosity may compromise fertilization, implantation, and/or embryonic development.

Nine out of 16 of the BK-D434G channelopathy patients had generalized epilepsy (13). These patients typically had absence seizures with SWDs. We therefore used simultaneous video-electroencephalogram (EEG) recording (Fig. 1*B* and *Methods*) to examine if the knock-in mice resemble the human BK-D434G patients' clinical manifestations (Table 1). We found that both the heterozygous $BK^{DG/WT}$ and homozygous $BK^{DG/DG}$ mice, but not the wild-type (WT) $BK^{WT/WT}$ control mice, exhibited frequent episodes of spontaneous, generalized SWDs, each of which lasted for 0.5 to 10 s (Fig. 1*C*, Table 1, and Movie S1). Power spectral analysis of the SWDs showed that the epileptic events of the BK-D434G mice were composed of strong frequency bands of 3 to 8 Hz (Fig. 1*D*), which is comparable to the typical SWD frequency range in other rodent models with absence seizures (Table 1) (36, 37). Compared with the $BK^{DG/WT}$ mice, which had 54.1 ± 13.4 SWDs per h, the homozygous $BK^{DG/DG}$ mice showed dramatically increased incidences of SWDs (263.7 ± 34.8 SWDs per h) (Fig. 1*E*).

We also observed frequent and prolonged immobilization phases in the BK-D434G mice during our video-EEG recordings (Movie S1 and Table 1). To unbiasedly detect and quantify the locomotor immobilization, we developed an automatic video analysis algorithm using a method similar to one reported previously (see *Methods* for details) (38). Using automated image segmentation (*SI Appendix*, Fig. S2*A*), we quantified animal total movement at 1-s interval and empirically defined total movement larger than 300 pixels as a locomotive event and less than 300 pixels as immobilization (*SI Appendix*, Fig. S2*B*). Different from the $BK^{WT/WT}$ mice that constantly underwent alternating locomotive and nonlocomotive status (Fig. 1 *Ci*), the $BK^{DG/WT}$ and $BK^{DG/DG}$ mice showed much higher incidences and prolonged durations of nonlocomotion (Fig. 1 *Cii* and *Ciii*), suggesting that the mutant animals had enhanced behavioral arrest, a hallmark of absence seizures (39). When aligning the locomotive activities with the SWDs, we found that when SWDs developed the mice were behaviorally arrested, whereas when the mice were spared from SWDs they were able to freely move around (Fig. 1*C* and Movie S1). All these data further support that the BK-D434G mice have frequent spontaneous absence seizures.

The BK-D434G proband responded to valproate (Table 1) (13). Therefore, we tested the effects of the first-line antiabsence medicines valproate and ethosuximide (ESM) on our BK-D434G mice. Given that the $BK^{DG/DG}$ mice have more robust and higher frequency of spontaneous absence seizures than the $BK^{DG/WT}$ mice (Fig. 1 *C–E*), we tested these medicines on the homozygous mice. Administration of valproate or ESM effectively suppressed the frequent SWDs in the animals for about an hour (*SI Appendix*, Fig. S3 and Fig. 1*F*). Typical SWDs accompanied by behavioral arrest and responsiveness to the first-line antiabsence seizure medicines (Table 1) explicitly demonstrated that the BK-D434G mice fully align with the clinical manifestations of absence epilepsy from the human patients carrying BK-D434G mutation (13).

BK-D434G Knock-In Mice Are Susceptible to Convulsant-Induced Tonic–Clonic Seizures. In addition to absence seizures, two BK-D434G channelopathy patients were also reported to

develop generalized tonic–clonic seizures (13). As no spontaneous generalized tonic–clonic seizures were observed in the naive BK-D434G mice, we hypothesized that BK-D434G GOF mutation may be susceptible to develop tonic–clonic seizures with external triggers. To test this, we administered pentylenetetrazole (PTZ) (40), a convulsant, to the $BK^{WT/WT}$ and $BK^{DG/WT}$ mice. We found that the low dosage of PTZ injection (40 mg/kg) induced generalized seizure (GS) stage (Racine seizure score ≥4; see *Methods* for details) in all $BK^{DG/WT}$ mice, whereas the same dosage of PTZ injection induced GS stage in only 42.9% of the $BK^{WT/WT}$ mice (*SI Appendix*, Fig. S4*A*). Furthermore, the $BK^{DG/WT}$ mice exhibited significantly increased seizure scores (*SI Appendix*, Fig. S4*A*), markedly prolonged GS duration (*SI Appendix*, Fig. S4*B*), and dramatically reduced latency to GS (*SI Appendix*, Fig. S4*C*). Our characterizations of the BK-D434G mice suggest that the BK GOF mutation not only can induce spontaneous absence seizures but also increases the vulnerability to develop generalized tonic–clonic seizures by external triggers.

Cortical Pyramidal Neurons of BK-D434G Mice Show Hyperexcitability. Cortical neurons play essential roles in the pathogenesis of absence seizures (32), and BK channels are highly expressed in cortical pyramidal neurons (2, 3). Therefore, we investigated whether BK-D434G GOF mutation alters the membrane excitability of cortical pyramidal neurons. Our acute brain slice recording showed that the pyramidal neurons of the layer V/VI of the somatosensory cortex from the $BK^{DG/WT}$ and $BK^{DG/DG}$ mice exhibited hyperexcitability as evidenced by the significantly increased overall AP frequency compared with the $BK^{WT/WT}$ mice (Fig. 2 *A* and *B* and *SI Appendix*, Table S1). This is consistent with the increased spontaneous SWDs in the homozygous mice (Fig. 1 *C–E*). Single AP analysis of the first spikes revealed that the BK-D434G cortical neurons exhibited much faster repolarization as evidenced by the significantly shortened AP duration (AP90) and augmented afterhyperpolarization amplitude (AHP), with the $BK^{DG/DG}$ neurons showing more dramatic changes (Fig. 2 *C–E*). Our analysis of the first 10 APs further demonstrated that the $BK^{DG/WT}$ neurons showed significantly shorter AP duration, enhanced AHP, larger AP amplitude, and higher firing frequency compared to the $BK^{WT/WT}$ neurons (*SI Appendix*, Fig. S5). All these observed electrophysiological property changes in the BK-D434G cortical neurons are consistent with BK-D434G's enhanced Ca^{2+} sensitivity (13, 33) and the well-documented notion that BK conductance mainly contributes to the fAHP phase of an AP (11, 12). Our in vitro electrophysiological characterizations thus demonstrated that the BK-D434G GOF mutant channels can more efficiently repolarize the membrane following membrane depolarization and VGCC opening so that the next spike can be readily generated.

Pharmacological Inhibition of BK Channels Suppresses BK-D434G–Induced Seizures. We next tested whether pharmacological inhibition of BK channels can restore normal firing and suppress absence seizures in the $BK^{DG/WT}$ and $BK^{DG/DG}$ mice. PAX, a BK channel-specific blocker (41), effectively suppressed the hyperexcitability of cortical pyramidal neuron (Fig. 3 *A* and *B* and *SI Appendix*, Table S1), markedly slowed down membrane repolarization, prolonged AP90, and reduced AHP amplitude (Fig. 3 *C–E*). Consistent with our brain slice recording, administration of PAX (0.35 mg/kg intraperitoneally [i.p.]) eliminated the spontaneous SWDs of the $BK^{DG/DG}$ mice and prevented their behavioral arrest for about 30 min (Fig. 3 *F–H*). Moreover, we found the PAX also decreased the severity of the PTZ-induced seizures in the heterogeneous $BK^{DG/WT}$ mice (*SI Appendix*, Fig. S6). Compared with the saline control, PAX administration significantly decreased seizure scores (*SI Appendix*, Fig. S6*A*), markedly reduced GS duration (*SI Appendix*, Fig. S6*B*), and dramatically prolonged the latency to GS (*SI Appendix*, Fig. S6*C*). All these are consistent with the anticonvulsant effect of PAX on the rodent models of epilepsy, including the PTZ-injected rodent models and an Angelman syndrome mouse model with enhanced BK channel activity (27, 42, 43). Our in vitro and in vivo experiments thus explicitly showed that pharmacological inhibition of BK channels can suppress absence seizures in the BK-D434G mice and reduce their vulnerability to convulsant-induced seizure.

BK-D434G Mice Exhibit Severe Locomotive Defects and Dyskinesia-Like Behaviors. In addition to absence epilepsy, the majority of the patients (12 out of 16) with BK-D434G mutation also had paroxysmal dyskinesia (Table 2) (13). We thus performed a battery of locomotor tests to assess the potential motor defects of the knock-in mice. We first used the open field test to evaluate their general locomotor activities (Fig. 4*A*). During a 15-min test, the total travel distance of the $BK^{DG/DG}$ mice was dramatically less than that of the $BK^{WT/WT}$ and $BK^{DG/WT}$ mice (Fig. 4*A*). Our balance beam test demonstrated that the $BK^{DG/DG}$ mice took significantly longer time to traverse the balance beam and had significant more incidences of hind-limb slips compared with the WT controls (Fig. 4*B* and Movie S2). The $BK^{DG/WT}$ mice showed no defect on transverse time yet had a milder defect on the number of hind-limb slips. Interestingly, the tails of the BK-D434G mice frequently wrapped around the beam to keep their balance when their hind limbs slipped (Movie S2). We next performed an accelerated rotarod test, which is a standard assay to evaluate impairment in rodent locomotor performance. Both the $BK^{DG/WT}$ and the $BK^{DG/DG}$ mice performed poorly on this more challenging motor task with significantly shorter latency to fall (Fig. 4*C* and Movie S3). Compared with the $BK^{DG/WT}$ mice, the $BK^{DG/DG}$ mice showed worse performance on rotarod. The severe defects observed during the accelerated rotarod test clearly showed that the BK-D434G mice indeed have impaired locomotor functions. Several factors such as muscle strength, motor learning, and motor coordination may affect rotarod performance (44). To specifically evaluate the motor coordination functions of the BK-D434G mice, we performed gait analysis utilizing footprints (Fig. 4*D*). We found that the $BK^{DG/DG}$ mice had significantly shorter hind-limb stride lengths than the $BK^{WT/WT}$ mice (Fig. 4*D*), suggesting that these mutant animals had severe defects on motor coordination.

While the BK-D434G mice displayed several locomotor abnormalities, we seldom observed spontaneous involuntary movements or abnormal postures, the clinical hallmark of paroxysmal dyskinesia, in the BK-D434G mice. Given the fact that the PNKD from the BK-D434G patients is not triggered by sudden movements or exercise but by alcohol, fatigue, and stress (13), we next tested whether alcohol or stress could induce dyskinesia behaviors in the BK-D434G mice. We found that low-dose ethanol (0.5 g/kg body weight, i.p.) can reliably trigger dyskinesia-like behaviors in the $BK^{DG/WT}$ and $BK^{DG/DG}$ mice but not their littermate WT controls (Fig. 4*E* and Movie S4). The involuntary dyskinesia-like behaviors are characterized by overextension of their hind paws. Next, we challenged the BK-D434G mice with the nonselective muscarinic receptor agonist oxotremorine, which was recently proved to trigger the dyskinesia/dystonia-like behavior in other genetic mouse models

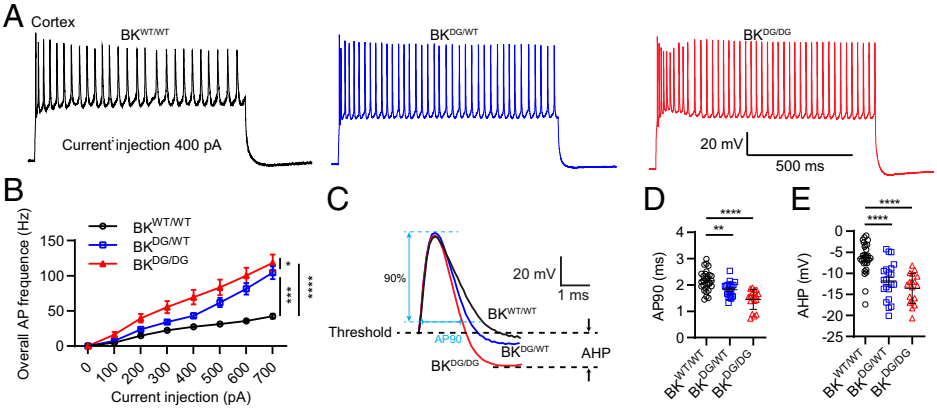

Fig. 2. Whole-cell electrophysiology shows that the BK-D434G cortical pyramidal neurons are hyperactive. (*A*) Representative evoked APs in layer V/VI pyramidal neurons of the somatosensory cortex from $BK^{WT/WT}$, $BK^{DG/WT}$, and $BK^{DG/DG}$ mice. Firing was elicited by a 400-pA current injection for 1 s. (*B*) Overall AP frequency from the $BK^{WT/WT}$, $BK^{DG/WT}$, and $BK^{DG/DG}$ cortical pyramidal neurons. Two-way repeated-measures ANOVA, $F_{(2,65)} = 25.59$, $P < 0.0001$. (*C*) Representative single AP waveforms elicited by 400-pA current injection. Definitions of AP parameters are labeled with cyan and black dashed lines. AP90 was used to define as AP duration of 90% repolarization and AHP denotes after hyperpolarization. (*D* and *E*) BK-D434G cortical neurons have shorter AP duration [*D*, one-way ANOVA test, $F_{(2,65)} = 22.35$, $P < 0.0001$] and higher amplitude of fast AHP [*E*, one-way ANOVA test, $F_{(2,65)} = 22.31$, $P < 0.0001$] compared with $BK^{WT/WT}$ neurons. $n = 29$ neurons from five $BK^{WT/WT}$ mice, $n = 21$ neurons from four $BK^{DG/WT}$ mice, and $n = 18$ neurons from four $BK^{DG/DG}$ mice. *$P < 0.05$, **$P < 0.01$, ***$P < 0.001$, ****$P < 0.0001$. In all plots and statistical tests, summary graphs show mean ± SEM.

(45, 46). Both the BK-D434G and WT control mice were injected with low-dose oxotremorine (0.01 mg/kg, i.p.) and observed for 1 h. The BK-D434G mice exhibited a dramatic reduction in spontaneous locomotion, prolonged time of immobility, and, more importantly, overextended hind paws, a typical dyskinesia-like behavior (Fig. 4*F* and Movie S5). On the other hand, the littermate WT mice only displayed mild reduction of spontaneous locomotion without detectable dyskinesia-like hind paw extension during the first 30 min, and they gradually recovered to normal locomotion 30 min after injection. A quantitative analysis, using the established scales for motor abnormalities in the mice (45, 46), clearly demonstrated the severe motor dysfunction in the BK-D434G mice in response to oxotremorine (Fig. 4*F*). Finally, after stressing the mice with a 30-s tail suspension, 3 out of 18 $BK^{DG/WT}$ mice and 3 out of 8 $BK^{DG/DG}$ mice displayed the limb-clasping behavior (Fig. 4*G* and Movie S6), whereas none of the 19 $BK^{WT/WT}$ mice showed this behavior. Taken together, our comprehensive behavioral characterizations demonstrated that the BK-D434G mice not only have severe locomotor deficiency but also tend to develop dyskinesia-like behaviors after ethanol or stress stimulation, a clinical feature observed in some of the BK-D434G patients (Table 2) (13).

Hyperexcitability of BK-D434G Cerebellar PCs. BK channels are highly expressed in PCs and play a critical role in controlling PC excitability (2). Genetic ablation of BK channels in murine PCs leads to cerebellar ataxia and impaired motor coordination (47, 48), and some *KCNMA1* channelopathy patients showed signs of cerebellar atrophy (15, 17–20). Given all these facts, we set out to examine whether BK-D434G GOF in PC contributes to the observed impairments in motor functions. By immunostaining with the PC marker calbindin, we found that the adult BK-D434G mutant mice showed dramatic changes of their PC morphology (Fig. 5*A*). The size of PC soma and the width of PC primary dendrites were significantly enlarged in both the $BK^{DG/WT}$ and the $BK^{DG/DG}$ mice compared with the $BK^{WT/WT}$ mice (Fig. 5 *B* and *C*), indicating signs of PC hypertrophy in the BK-D434G mice.

Next, we conducted brain slice patch-clamp recording on the PCs from the BK-D434G and WT control mice (Fig. 5 *D*–*K*). We found the membrane capacitance (Cm) of the BK-D434G PCs was significantly larger than that of the WT control (Fig. 5*D* and *SI Appendix*, Table S1). As Cm is proportional to cell surface area, our Cm measurement is thus consistent with our morphological estimation using immunostaining (Fig. 5 *A*–*C*), both of which demonstrated abnormally enlarged somatodendritic sizes in the BK-D434G PCs (Fig. 5 *A* and *B*). By measuring the spontaneous firing rate in the PCs, we found that the BK-D434G mice had significantly higher spontaneous firing frequencies than the WT control (Fig. 5 *E* and *F*). Next, upon current injection, similar to what we observed in cortical pyramidal neurons (Fig. 3 *A*–*E*), we found that the $BK^{DG/WT}$ PCs had dramatically enhanced firing rate compared with the PCs of the $BK^{WT/WT}$ mice (Fig. 5 *G* and *H*). The subsequent single AP waveform analysis showed that the BK-D434G PCs showed accelerated membrane repolarization (Fig. 5*I*) with significant reduction of AP duration (Fig. 5*J*) and increase of AHP amplitude (Fig. 5*K*). The $BK^{DG/DG}$ PCs always showed greater changes than the $BK^{DG/WT}$ PCs, consistent with the more dramatic locomotor defects observed in the homozygous mice (Fig. 4).

Blocking BK Reduces the Hyperactivity of the PCs and Alleviates the Motor Defects of the BK-D434G Mice. Consistent with our observations in the cortical pyramidal neurons (Fig. 3 *A*–*E*), application of 10 μM PAX robustly reversed the changes of single AP waveform caused by the BK-D434G mutation and efficiently suppressed the hyperactive PCs in the BK-D434G mice (Fig. 6 *A*–*E* and *SI Appendix*, Table S1). We next tested whether pharmacological inhibition of BK by PAX can restore the locomotor deficiency in the BK-D434G mice. We found that the administration of PAX (0.35 mg/kg i.p.) can rescue the motor impairments in the $BK^{DG/WT}$ mice, partially in the $BK^{DG/DG}$ mice evaluated by the open field, rotarod, balance beam, and gait tests (Fig. 6 *F*–*I*). Our data thus suggest that BK inhibition could be a potential strategy to alleviate BK GOF-induced locomotor deficiency.

Discussion

In this study we show that the BK-D434G knock-in mice fully resemble the clinical manifestations of generalized absence epilepsy and PNKD observed in the BK-D434G patients (Tables 1 and 2) (13). The BK-D434G mice exhibited spontaneous SWDs, which can be suppressed by the first line antiabsence medicines and a BK channel-specific blocker, PAX. In addition, we reliably observed PNKD-like involuntary movement when the animals were challenged with ethanol or stress, a clinical feature reported in some of the BK-D434G patients (13). Our findings not only indicated that BK-D434G GOF played an important role in absence epilepsy and PNKD but also demonstrated pharmacological inhibition of BK conductance as a

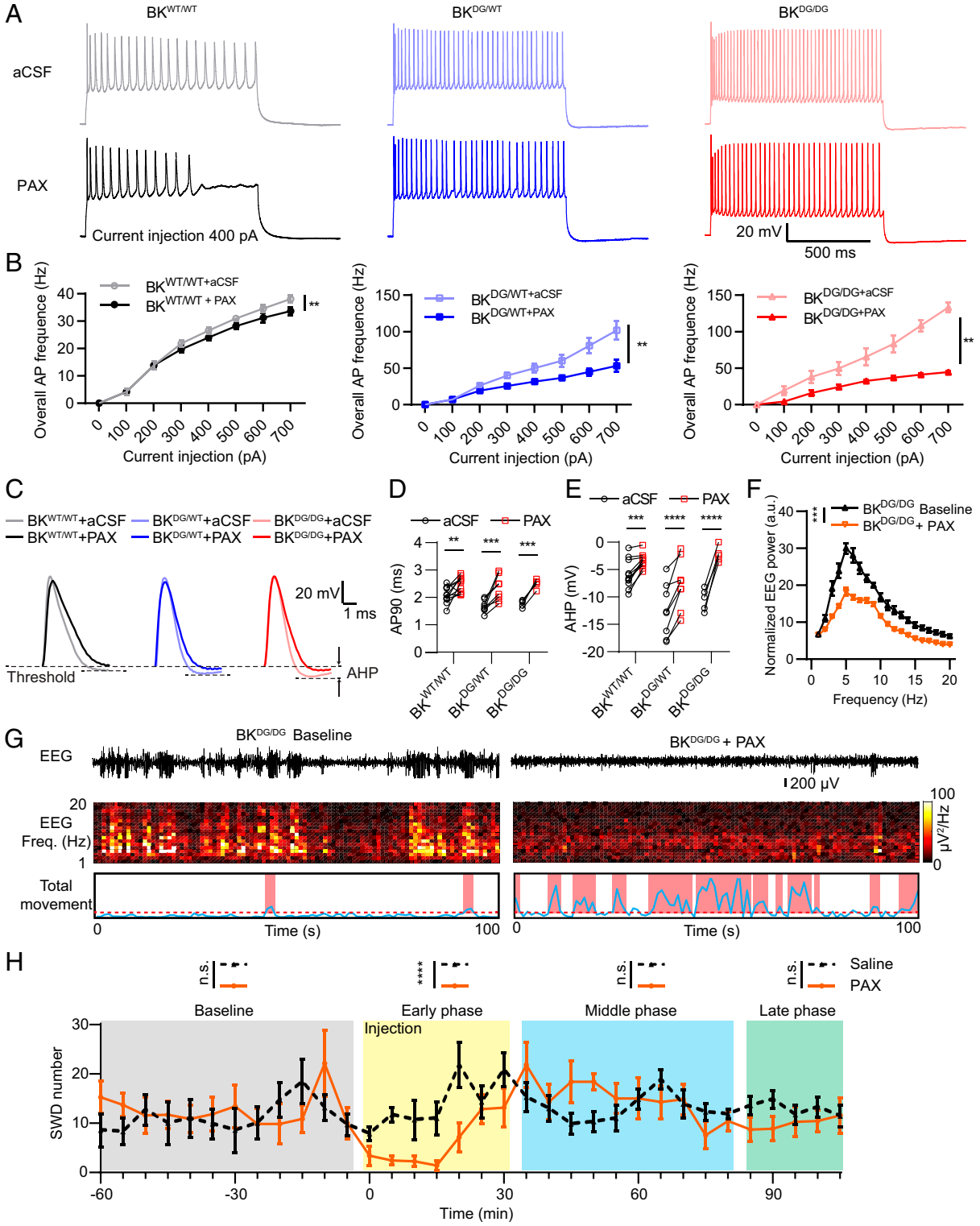

Fig. 3. PAX, a BK channel blocker, reduces the hyperactivity of the cortical pyramidal neurons and suppresses the spontaneous absence seizures of the BK-D434G mice. (*A*) Representative evoked APs in layer V/VI pyramidal neurons of the somatosensory cortex from $BK^{WT/WT}$, $BK^{DG/WT}$, and $BK^{DG/DG}$ mice. Firing was elicited by 1-s, 400-pA current injection, before and after application of 10 µM PAX. (*B*) Overall AP frequency from the $BK^{WT/WT}$, $BK^{DG/WT}$, and $BK^{DG/DG}$ cortical pyramidal neurons before and after application of PAX [two-way repeated-measures ANOVA, $BK^{WT/WT}$, $F_{(1,15)} = 12.77$, $P = 0.0028$. $n = 16$ neurons from five mice; $BK^{WT/DG}$, $F_{(1,10)} = 10.27$, $P = 0.0084$. $n = 11$ neurons from three mice; $BK^{DG/DG}$, $F_{(1,4)} = 24.95$, $P = 0.0075$. $n = 5$ neurons from two mice]. (*C*) Representative single AP waveforms of the $BK^{WT/WT}$, $BK^{DG/WT}$, and $BK^{DG/DG}$ cortical neurons elicited by 400-pA current injection before and after application of PAX. (*D* and *E*) PAX broadens AP duration [*D*, two-way repeated-measures ANOVA, $F_{(1,21)} = 160.8$, $P < 0.0001$] and suppresses after-hyperpolarization (AHP) in the cortical pyramidal cells from $BK^{WT/WT}$, $BK^{DG/WT}$, and $BK^{DG/DG}$ mice [*E*, two-way repeated-measures ANOVA, $F_{(1,21)} = 54.41$, $P < 0.0001$]. (*F*) Summary of power spectral density of EEG recorded from $BK^{DG/DG}$ mice before and after PAX administration ($n = 7$ mice). Two-way ANOVA, $F_{(1,12)} = 26.39$, $P = 0.0002$. $n = 7$ mice. (*G*) Representative EEG traces, corresponding spectrograms, and total movement from the $BK^{DG/DG}$ mice before (*Left*) and after (*Right*) 0.35 mg/kg PAX administration. (*H*) Time course of the drug effects of PAX (orange line) and saline control (black dash line) on the spontaneous SWDs of the $BK^{DG/DG}$ mice (bin size = 5 min). PAX is effective in the early phase, 30 min postinjection [yellow box, two-way repeated-measures ANOVA, $F_{(1,12)} = 42.57$, $P < 0.0001$] but not in the later phases. $n = 7$ mice per group. The error bars indicate SEM; $^{**}P < 0.01$, $^{***}P < 0.001$, $^{****}P < 0.0001$. n.s., not statistically significant. In all plots and statistical tests, summary graphs show mean ± SEM.

Table 2. Comparison of motor phenotypes in BK-D434G patients and mice

	BK-D434G proband	BK-D434G mouse
Onset of the paroxysmal dyskinesia		
Triggered by sudden movement	–	–
Triggered by stress	+	Some of the mice
Triggered by alcohol	+	+
Other locomotor activities		
Reduction of locomotor activity	N/A	+
Reduction of coordination and balance	N/A	+
Gait	N/A	+
Ref.	13	Current study

N/A: not applicate or not available.

promising therapeutic strategy to mitigate BK-GOF induced epilepsy and dyskinesia.

Utilizing the BK-D434G knock-in mice, we attempted to uncover the cellular pathophysiology of the GOF BK mutation in inducing epilepsy and dyskinesia. We decided to choose cortical pyramidal neurons and cerebellar PCs as two model neurons to tackle this question because 1) they are known to be important for the pathogenesis of absence seizures and dyskinesia, respectively (32, 39, 45, 49, 50) and 2) BK channels are highly expressed in these neurons (2, 3). We found that BK-D434G causes hyperexcitability in both neurons. Given that BK channels usually form protein complexes with VGCCs (Fig. 1*A*) in the central nervous system (9), BK-D434G GOF mutation with enhanced Ca^{2+} sensitivity is expected to be rapidly activated following membrane depolarization and Ca^{2+} entry from the VGCCs. The enhanced BK channel-mediated K^+ efflux robustly accelerates AHP as evidenced by significant shortening of ADP90 (Fig. 2 *C* and *D* and *SI Appendix*, Fig. S5 *I* and *J*) and enhanced amplitude of AHP (Fig. 2 *C* and *E* and *SI Appendix*, Fig. S5 *I* and *K*). The enhanced AHP would rapidly reprime of the inactivated voltage-gated sodium channels (*SI Appendix*, Fig. S5 *A*, *B*, and *F*) and/or promote the activation of hyperpolarization-activated cation channels, all of which could collectively promote the BK-D434G cortical neurons and PCs to fire at a higher frequency (11, 51). Although detailed cellular model of BK-D434G-induced neuronal hyperexcitability warrants future experimental and computational studies, the consistency of our current finding and a recent electrophysiological recording of the large ventral lateral neurons from a BK-D434G mutant *Drosophila* model (23) clearly demonstrate the importance of BK GOF on modulating neuronal excitability. Characterizations of different BK GOF mouse models will help further understand BK channel's contributions to neuronal activities and neurological disorders (52).

Abnormal oscillatory rhythms within the cortico-thalamic system are generally believed to be responsible for absence seizure ictogenesis (32, 39, 49). The hyperexcitability of BK-D434G cortical pyramidal neurons observed in this study supports the importance of cortical excitability in absence seizure pathogenesis. Future studies need to be done to comprehensively characterize the excitabilities of the different types of neurons in the cortico-thalamic system and illustrate the circuit basis of absence seizure ictogenesis in the BK-D434G mice.

It is interesting to observe that GABAergic PCs from the BK-D434G mice are also hyperactive, as evidence by significantly increased spontaneously and evoked firing (Fig. 5 *E*–*H*). One of the initial proposals to explain BK GOF-induced overall hyperexcitability in the brain is that the GOF mutations would suppress inhibitory neurons and reduce GABA release, thereby leading to disinhibition of neuronal networks and subsequently hyperexcitability (13). Our observation of higher firing frequency in the BK-D434G PCs suggests that the inhibitory neurons with high expression of BK GOF mutations, instead of reducing their excitability, would increase their excitability in the somatodendritic region. In the future, it is critical to elucidate the contributions BK GOF to membrane excitability in other inhibitory neurons and the effects of BK GOF on inhibitory synaptic transmission.

In addition to having spontaneous absence seizures (Fig. 1 *C*–*F*), the BK-D434G mice are also more susceptible to PTZ-induced tonic–clonic seizures (*SI Appendix*, Fig. S4). It is likely that BK-D434G GOF may also enhance the excitability of the other neurons outside of the cortico-thalamic system such as hippocampal pyramidal neurons and dentate gyrus granule cells (12). Future investigations of the excitabilities of these neurons from the BK-D434G mice will shine light on understanding the neuronal and circuit basis of developing tonic–clonic seizures in some of the refectory and/or pharmacoresistant absence seizure patients (53).

Despite clinical applications of the first-line antiabsence medicines including ESM and valproate since the 1950s (54–56), 30% of absence epilepsy patients are pharmacoresistant and 60% of them are affected by severe neuropsychiatric comorbidities, including attentional, mood, cognitive, and memory impairments (32, 57). While human genetics and animal models have shown that VGCCs and $GABA_A$ receptor chloride channels contribute to the etiology of absence epilepsy (39, 58, 59), the contributions of potassium channels to absence epilepsy pathogenesis are still elusive. In this study, we showed that PAX, a BK channel blocker, can effectively suppress BK-D434G–induced hyperexcitability and absence seizures (Fig. 3), as well as PTZ-induced tonic–clonic seizures (*SI Appendix*, Fig. S6). This is consistent with the previous findings that PAX can alleviate convulsant drug-induced generalized epilepsy (42, 43) and spontaneous seizures in an Angelman syndrome mouse model with enhanced BK channel activity (27). Our current study thus demonstrated that targeting BK channels could be a novel strategy to mitigate absence epilepsy. Future investigations are needed to examine if pharmacological inhibition of BK channels can be a general strategy to treat different BK GOF channelopathy and could be used to treat pharmaco-resistant absence epilepsy. Of course, better BK inhibitors also need to be developed because PAX's antiabsence effect vanishes in 30 min after injection due to its poor pharmacokinetics (Fig. 3*H*) (60).

The BK-D434G mice showed severe locomotor defects as examined using open field, balance beam, rotarod, and gait analysis (Fig. 4 *A*–*D*). When compared with the *Drosophila*

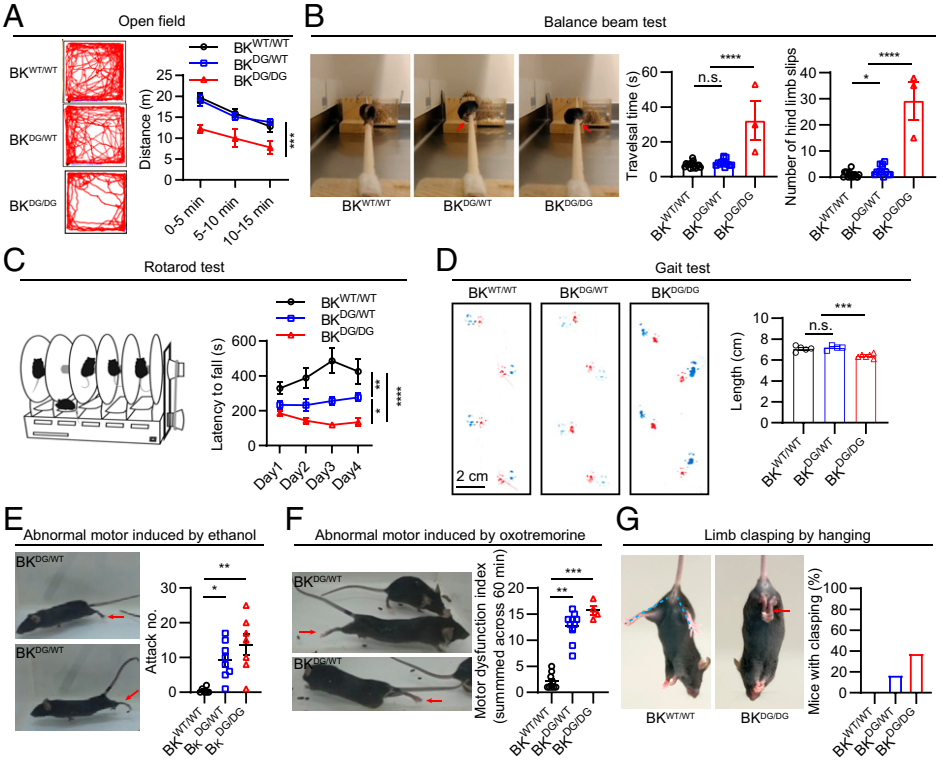

Fig. 4. BK-D434G mice exhibit motor defects and dyskinesia-like behaviors. (*A*, *Left*) Representative animal tracks in the open-field chamber of $BK^{WT/WT}$, $BK^{DG/WT}$, and $BK^{DG/DG}$ mice. (*Right*) $BK^{DG/DG}$ mice showed decreased locomotor activity in 15-min open field test. Two-way repeated-measures ANOVA, $F_{(2,23)} = 9.974$, $P = 0.0008$. $BK^{WT/WT}$, $n = 9$ mice; $BK^{DG/WT}$, $n = 12$ mice; $BK^{DG/DG}$, $n = 5$ mice. (*B*) Balance beam test of BK-D434G mutation mice. (*Left*) The red arrows indicate the low position of the tails when hind-limb slips caused balance loss were observed during the test. $BK^{DG/DG}$ mice had significantly more hind-limb slips on the balance beams [*Middle*, one-way ANOVA test, $F_{(2,27)} = 75.05$, $P < 0.0001$] and took significantly longer to traverse the balance beam [*Right*, one-way ANOVA test, $F_{(2,27)} = 27.14$, $P < 0.0001$] compared with $BK^{WT/WT}$ controls. $BK^{WT/WT}$, $n = 15$ mice; $BK^{DG/WT}$, $n = 12$ mice; $BK^{DG/DG}$, $n = 3$ mice. (*C*) Accelerating rotarod latency to fall times for BK-D434G mutation mice over 4 d of testing compared with control mice, showing a significant deficit for BK-D434G mice in this test. Two-way repeated-measures ANOVA, $F_{(2,28)} = 19.56$, $P < 0.0001$. $BK^{WT/WT}$, $n = 8$ mice; $BK^{DG/WT}$, $n = 12$ mice; $BK^{DG/DG}$, $n = 11$ mice. (*D*, *Left*) Representative images of the gait patterns of the $BK^{WT/WT}$, $BK^{DG/WT}$, and $BK^{DG/DG}$ mice, with forepaws represented by red paint and hind paws by blue paint. (Scale bar, 2 cm.) (*D*, *Right*) Quantification reveals shortened stride length. One-way ANOVA test, $F_{(2,12)} = 18.50$, $P = 0.0002$. $BK^{WT/WT}$, $n = 6$ mice; $BK^{DG/WT}$, $n = 8$ mice; $BK^{DG/DG}$, $n = 7$ mice. (*E*) Ethanol-induced dyskinesia-like behaviors. (*Left*) Representative images of dyskinesia-like behaviors (overextension of hind paws, red arrows) triggered by ethanol (0.5 g/kg body weight, i.p.). (*Right*) Dyskinesia-like attack numbers of $BK^{WT/WT}$, $BK^{DG/WT}$, and $BK^{DG/DG}$ mice after ethanol injection. Kruskal–Wallis test (also called the "one-way ANOVA on ranks"), $P = 0.0008$. $BK^{WT/WT}$, $n = 5$ mice; $BK^{DG/WT}$, $n = 4$ mice; $BK^{DG/DG}$, $n = 6$ mice. (*F*) Oxotremorine-induced abnormal motor behaviors. (*Left*) Representative images of dyskinesia-like behaviors (overextension of hind paws, red arrows) triggered by oxotremorine (muscarinic acetylcholine receptor agonist, 0.01 mg/kg body weight, i.p.). (*Right*) Summed abnormal motor scores (see *Methods*) of $BK^{WT/WT}$, $BK^{DG/WT}$, and $BK^{DG/DG}$ mice after oxotremorine injection for 60 min. Kruskal–Wallis test, $P = 0.0001$. $BK^{WT/WT}$, $n = 9$ mice; $BK^{DG/WT}$, $n = 10$ mice; $BK^{DG/DG}$, $n = 4$ mice. (*G*) Tail suspension test. (*Left*) Representative images of a $BK^{WT/WT}$ mouse (*Left*) and a $BK^{DG/DG}$ mouse (*Right*) during the tail suspension. The blue dashed line demarcates the normal posture of hind limbs of the $BK^{WT/WT}$ mouse and the red arrow points to the limb clasping in the $BK^{DG/DG}$ mouse. (*Right*) Percentage of $BK^{WT/WT}$, $BK^{DG/WT}$, and $BK^{DG/DG}$ mice displaying limb clasping in the 30-s tail suspension test. $BK^{WT/WT}$, $n = 19$ mice; $BK^{DG/WT}$, $n = 18$ mice; $BK^{DG/DG}$, $n = 8$ mice. In all plots and statistical tests, summary graphs show mean ± SEM; $^*P < 0.05$, $^{**}P < 0.01$, $^{***}P < 0.001$, $^{****}P < 0.0001$. n.s., not statistically significant.

model that carries the same mutation, both BK-D434G models exhibited significant reduction of the total travel distance (23). The BK-D434G mice rarely exhibited spontaneous paroxysmal dyskinesia during our observation window. Nevertheless, ethanol, oxotremorine, or stress by tail suspension can prominently induce the dyskinesia/dystonia-like behaviors in the mutated mice (Fig. 4 *E*–*G* and Movies S4–S6). This is consistent with the clinical observations that PNKD can be trigged by ethanol or stress (13). In the current study, we also discovered that the PCs from the BK-D434G mice exhibited hyperexcitability and morphological changes (Fig. 5). In agreement with our findings, the abnormally increased firing of PCs has been reported to be tightly correlated with paroxysmal dyskinesia in several dystonia mouse models (61, 62), which is characterized by sudden extension of their trunk and limbs. Another mouse model with hyperactivation of the mTORC1 also causes PC hypertrophy and impaired motor performance (63). In addition, we recently discovered that a dystonia/atonia patient who carries another BK GOF mutation, N536H, exhibited mild cerebellar atrophy (17). Taken together, previous reports and our current finding strongly support the involvement of the cerebellum in dyskinesia/dystonia pathogenesis. As the alterations of the basal ganglia circuitries are well-established to contribute to the pathogenesis of dyskinesia, especially the levodopa (L-DOPA)–induced dyskinesia (64, 65), it is critical to further investigate the BK-D434G effects on the basal ganglia and cerebellar functions in vitro and in vivo in future studies.

Although we demonstrated the effectiveness of BK inhibition using the highly potent BK inhibitor PAX (0.35 mg/kg) on suppressing absence seizures and improving locomotor performance, caution needs to be taken to directly translate PAX into clinical applications. First, the half-life of PAX is short, only lasting about 40 min inside the body (60). Second, PAX, when used at high dose (~8 mg/kg), can induce severe tremor and impair locomotor functions in animals (66). This highlights the urgent need to develop novel BK channel inhibitors with better pharmacokinetics and fewer side effects.

Taken together, the BK-D434G knock-in mice, a mouse model carrying a human BK channel mutation, fully resembled the clinical manifestations of human patients with absence seizures and PNKD. Our current characterizations of this mouse model help advance our understanding of the pathophysiology of BK GOF in neurological disorders, shine new light on uncovering the mechanistic underpinnings of absence epilepsy and PNKD, and inspire developing novel therapeutics to treat these neurological disorders.

Methods

Mice. The BK-D434G mutation mice were generated by homologous recombination in embryonic stem cells and implanted in C57BL/6J blastocysts using standard procedures. The targeting vector was designed to flank the D434G mutation with a neomycin (Neo) selection cassette with loxP sites after exon 10 of the *KCNMA1* gene (*SI Appendix*, Fig. S1*A*). Chimeric mice were crossed to C57BL/6J

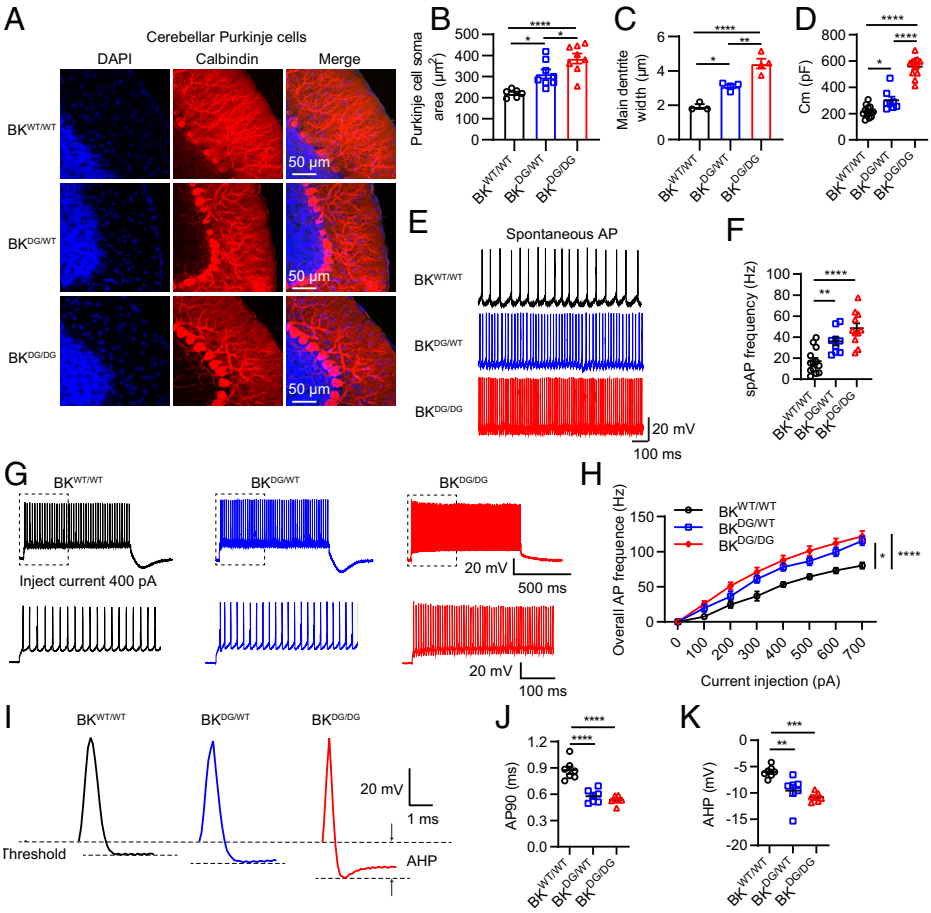

Fig. 5. Cerebellar PCs from the BK-D434G mutant mice are hyperactive. (*A*) Representative confocal images of PCs. The PCs from the $BK^{DG/WT}$ and $BK^{DG/DG}$ mice show signs of hypertrophy. (*B*) The $BK^{DG/WT}$ and $BK^{DG/DG}$ mice have enlarged PC somas. One-way ANOVA test, $F_{(2,19)} = 14.97$, $P = 0.0001$; $BK^{WT/WT}$, $n = 6$; $BK^{DG/WT}$, $n = 8$; $BK^{DG/DG}$, $n = 8$. (*C*) The $BK^{DG/WT}$ and $BK^{DG/DG}$ mice have thickened main dendrite width. The dendrite width is measured at the distance of one cell-soma diameter from the cell soma. One-way ANOVA test, $F_{(2,8)} = 34.46$, $P = 0.0001$, $BK^{WT/WT}$, $n = 3$; $BK^{DG/WT}$, $n = 4$; $BK^{DG/DG}$, $n = 4$. (*D*) The PCs from the $BK^{DG/WT}$ and $BK^{DG/DG}$ mice have increased Cm. One-way ANOVA test, $F_{(2,31)} = 96.92$, $P < 0.0001$; $BK^{WT/WT}$, $n = 14$; $BK^{DG/WT}$, $n = 8$; $BK^{DG/DG}$, $n = 12$. (*E*) Representative traces of spontaneous APs in the PCs from the $BK^{WT/WT}$, $BK^{DG/WT}$, and $BK^{DG/DG}$ mice. (*F*) The PCs from the $BK^{DG/WT}$ and $BK^{DG/DG}$ mice showed increased spontaneous firing frequency. One-way ANOVA test, $F_{(2,30)} = 17.53$, $P < 0.0001$; $BK^{WT/WT}$, $n = 13$; $BK^{DG/WT}$, $n = 9$; $BK^{DG/DG}$, $n = 11$. (*G*) Representative evoked APs in cerebellar PCs from $BK^{WT/WT}$, $BK^{DG/WT}$, and $BK^{DG/DG}$ mice. Firing was elicited by 1-s-long 400-pA current injection. (*Bottom*) Black dashed rectangles show the corresponding traces on an expanded time scale. (*H*) Overall AP frequency of the PCs from the $BK^{WT/WT}$, $BK^{DG/WT}$, and $BK^{DG/DG}$ mice. Two-way repeated-measures ANOVA, $F_{(2,23)} = 8.457$, $P = 0.0018$. $BK^{WT/WT}$, $n = 7$; $BK^{DG/WT}$, $n = 7$; $BK^{DG/DG}$, $n = 12$. (*I*) Representative single AP waveforms elicited by 400-pA current injection for $BK^{WT/WT}$, $BK^{DG/WT}$, and $BK^{DG/DG}$ mice. The black dashed lines denote the AP threshold and afterhyperpolarization (AHP). (*J* and *K*) BK-D434G PCs have shorter AP duration [*J*, one-way ANOVA test, $F_{(2,18)} = 35.90$, $P < 0.0001$] and higher amplitude of fast AHP [*K*, one-way ANOVA test, $F_{(2,18)} = 13.65$, $P = 0.0002$] compared with $BK^{WT/WT}$ neurons. $n = 7$ neurons from three $BK^{WT/WT}$ mice, $n = 7$ neurons from three $BK^{DG/WT}$ mice, and $n = 7$ neurons from three $BK^{DG/DG}$ mice. $^*P < 0.05$, $^{**}P < 0.01$, $^{***}P < 0.001$, $^{****}P < 0.0001$. In all plots and statistical tests, summary graphs show mean ± SEM.

females (000664; The Jackson Laboratory). Germline transmission generated heterozygous $BK^{D434G}BK^{+}$ ($BK^{DG/WT}$) mice. Germline transmission was determined by genotyping PCR of mouse tail DNA (*SI Appendix*, Fig. S1*B*), using primers *pKCNMA1*_genotyping F1 (5′-GTGCCTAGAGGTGGCTGGGAATTAG-3′) and *pKCNMA1*_genotyping R1 (5′-CCTCTCCTACGGTGGTAAAGTATCC-3′) for the WT allele (342 base pairs, bp) and the floxed allele (455 bp). The F1 hybrids were crossed to C57BL/6J β-actin Cre mice to excise the Neo cassette. The D434G mutations were confirmed by primers *pKCNMA1*_sequencing F2 (5′-GCTGAGTGGGGAGATGTATTGCTTC-3′) and *pKCNMA1*_sequencing R2 (5′-ACCTAAGGAGCCAGCACCAATCAT-3′). The BK-D434G mice were then back-crossed to C57BL/6J mice for five generations.

For all experiments, $BK^{DG/WT}$ males were bred with $BK^{DG/WT}$ females. Animals were housed at a constant 24 °C in a 12 h light–dark cycle (lights on at 7:00 AM) with ad libitum access to food and water. Both males and females were used for in vivo and in vitro analysis. Mouse handling and usage were carried out in a strict compliance with protocols approved by the Institutional Animal Care and Use Committee at Duke University, in accordance with National Institutes of Health guidelines. PCR genotyping was performed using tail DNA extraction at the birth of the mice.

Simultaneous Video-EEG Recording and Analysis. Mice ages 1 to 6 mo were anesthetized with 1∼2% isoflurane and mounted on a stereotaxic device (Kopf Instruments). A mouse EEG headstage (8201; Pinnacle Technology Inc.) was affixed to the skull with two screws, which served as recording leads on the parietal cortex (from the bregma: 1.50 mm posterior, 2.50 mm lateral) and cerebellar cortex (from the lambda: 1.50 mm posterior, 1.50 mm lateral). The headstage was subsequent secured to the skull by the super glue (Loctite Inc.) and dental cement and the animal could recover for 5 d prior to EEG recording. EEG recordings were collected by a preamplifier with 100× gain and high-pass-filtered at 1.0 Hz (8200-SE; Pinnacle Technology Inc.), accompanied by spontaneous video monitoring on the top of the chamber (Logitech C920 HD Pro Webcam, 24 frames per second). On the day of recording, the animals were habituated in the recording room for >1 h before the experiment. Data were acquired with an analog-to-digital converter (PCI-6221; National Instruments) to a desktop computer. A custom code written in MATLAB (MathWorks) was used to visualize the raw EEG recording trace and plot the power spectra using the Fast Fourier Transform within the frequency range of 1 to 20 Hz. The numbers of SWD events were calculated using previously described methods (67).

Video-Based Motion Analysis. The video-based motion was analyzed using a method similar to one previously described (38). A custom-written MATLAB code was used to analyze the video recordings of freely moving mice in the EEG recording chamber. The videos were first down-sampled to 1 frame per second and then converted to gray 8-bit images (*SI Appendix*, Fig. S2 *A*, *Upper*). Since the mouse is darker than the background in the gray images, we conducted the image segmentation (I_{seg_t}) of the mouse at time t by

$$I_{seg_t}(x_0, y_0)\begin{cases} 1, I_{seg_t}(x_0, y_0) < \mu \\ 0, I_{seg_t}(x_0, y_0) > \mu \end{cases},$$

where (x_0, y_0) is the coordinate of the image and μ is the threshold, the value of which was empirically set to be 10% of the darkest intensity (255) of the 8-bit image. A representative result of the segmentation images is shown in *SI Appendix*, Fig. S2 *A*, *Middle*.

To get the total movement of the mice over time, we obtained a subtracted image (I_{sub_t}) by substrating two sequential frames,

$$I_{sub_t}(x_0, y_0) = I_{sub_{t+1}}(x_0, y_0) - I_{seg_t}(x_0, y_0),$$

where $I_{seg_{t+1}}$ is the next sequential frame of I_{seg_t}. The subtracted images were shown in *SI Appendix*, Fig. S2 *A*, *Bottom*. Pixels changed above the empirical threshold (300 pixels) were designated as a motion status.

PTZ-Induced Seizure Model. We performed i.p. injection of 40 mg/kg PTZ (P6500; Sigma) and then immediately placed animals in a chamber and started video recording. PTZ-induced seizures were scored according to a modified Racine

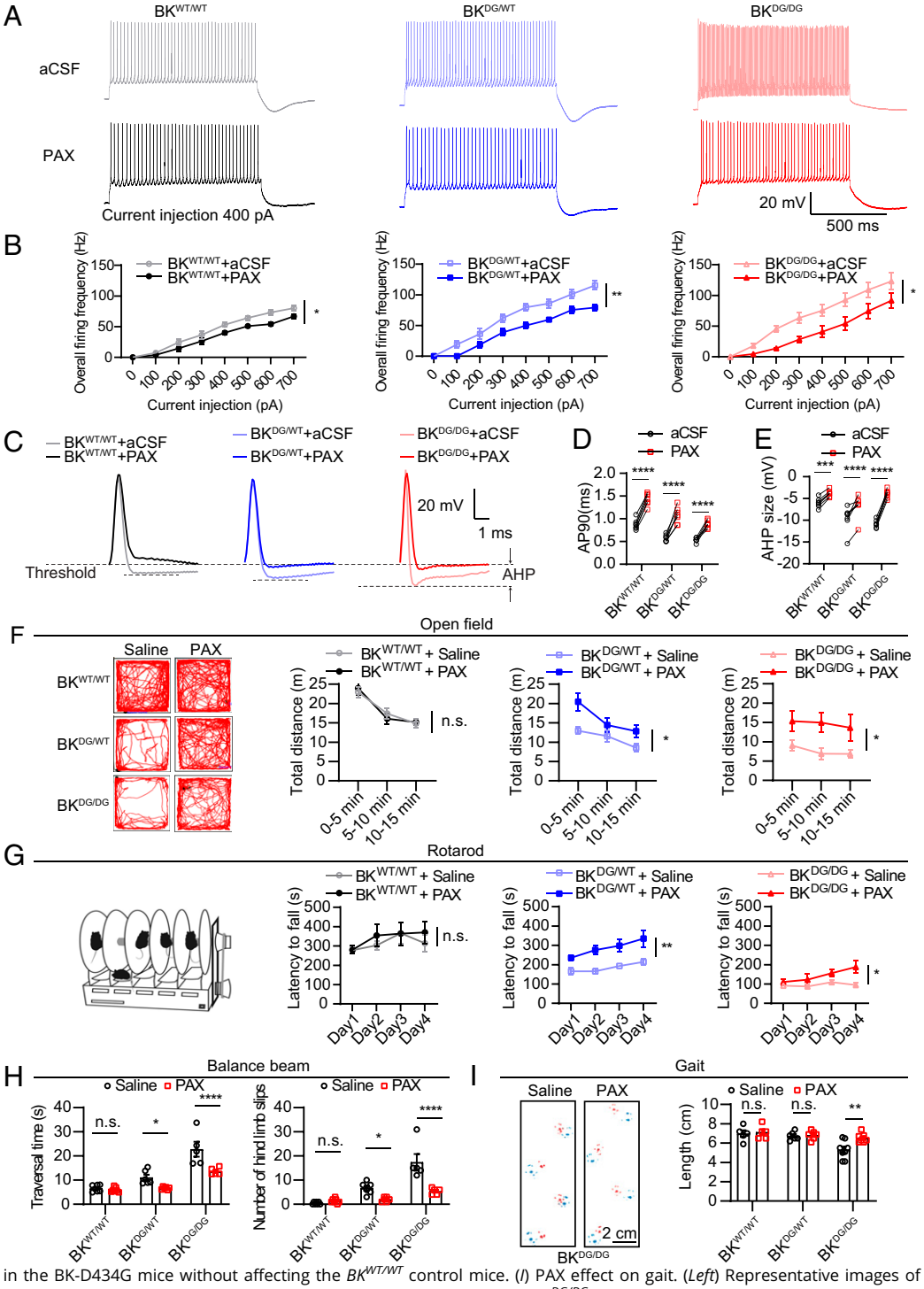

Fig. 6. PAX reduces the hyperactivity of the PCs and alleviates the motor defects of the BK-D434G mice. (*A*) Representative evoked APs in cerebellar PCs from $BK^{WT/WT}$, $BK^{DG/WT}$, and $BK^{DG/DG}$ mice. Firing was elicited by 1-s-long 400-pA current injection, before and after application of 10 μM PAX. (*B*) Overall AP frequency from the $BK^{WT/WT}$, $BK^{DG/WT}$, and $BK^{DG/DG}$ PCs before and after application of PAX [two-way repeated-measures ANOVA; $BK^{WT/WT}$, $F_{(1,12)} = 6.245$, $P = 0.0280$, $n = 7$ neurons from three mice; $BK^{WT/DG}$, $F_{(1,12)} = 15.68$, $P = 0.0022$, $n = 7$ neurons from three mice; $BK^{DG/DG}$, $F_{(1,12)} = 8.735$, $P = 0.0120$, $n = 7$ neurons from three mice]. (*C*) Representative single AP waveforms elicited by 400-pA current injection for $BK^{WT/WT}$, $BK^{DG/WT}$, and $BK^{DG/DG}$ mice before and after 10 μM PAX. The black dashed lines denote the AP threshold and AHP. (*D* and *E*) BK-D434G PCs have shorter AP duration (AP90) and higher amplitude of fAHP compared with $BK^{WT/WT}$. PAX broadens AP duration [*D*, two-way ANOVA, $F_{(1,18)} = 353.2$, $P < 0.0001$] and reduces fAHP [*E*, two-way ANOVA, $F_{(1,18)} = 228.7$, $P < 0.0001$] of PCs from both $BK^{WT/WT}$ and $BK^{DG/WT}$ mice. $BK^{WT/WT}$, $n = 7$ neurons from three mice; $BK^{WT/DG}$, $n = 7$ neurons from three mice; $BK^{DG/DG}$, $n = 7$ neurons from three mice. (*F*) PAX effect on open field test. (*Left*) Representative animal track in the open-field chamber of $BK^{WT/WT}$, $BK^{DG/WT}$, and $BK^{DG/DG}$ mice injected with PAX (0.35 mg/kg i.p.) or saline control. Two-way repeated-measures ANOVA; $BK^{WT/WT}$, $F_{(1,18)} = 0.0001$, $P = 0.9936$; $BK^{DG/WT}$, $F_{(1,14)} = 5.748$, $P = 0.0310$; $BK^{DG/DG}$, $F_{(1,12)} = 7.025$, $P = 0.0212$. (*G*) PAX effect on rotarod. PAX increases the latency to fall in the accelerating rotarod test from the BK-D434G mice, while the same concentration of PAX does not affect the $BK^{WT/WT}$ mice. Two-way repeated-measures ANOVA; $BK^{WT/WT}$, $F_{(1,118)} = 0.2202$, $P = 0.6445$; $BK^{DG/WT}$, $F_{(1,16)} = 14.40$, $P = 0.0016$; $BK^{DG/DG}$, $F_{(1,10)} = 4.966$, $P = 0.05$. (*H*) PAX effect on balance beam. PAX reduces the traversal time [*Left*, two-way ANOVA, $F_{(1,30)} = 25.16$, $P < 0.0001$] and number of hind-limb slips [*Right*, two-way ANOVA, $F_{(1,30)} = 22.69$, $P < 0.0001$] in the BK-D434G mice without affecting the $BK^{WT/WT}$ control mice. (*I*) PAX effect on gait. (*Left*) Representative images of the gait patterns of the $BK^{DG/DG}$ mice treated with saline or PAX. (*Right*) PAX rescues the gait length in the $BK^{DG/DG}$ mice; two-way ANOVA, $F_{(1,31)} = 4.746$, $P = 0.0371$. $^*P < 0.05$, $^{**}P < 0.01$, $^{***}P < 0.001$, $^{****}P < 0.0001$. n.s., not statistically significant. In all plots and statistical tests, summary graphs show mean ± SEM.

scale (68, 69): 0, normal behavior, no abnormality; 1, immobilization, lying on belly; 2, head nodding, facial, forelimb, or hindlimb myoclonus; 3, continuous whole-body myoclonus, myoclonic jerks, tail held up stiffly; 4, rearing, tonic seizure, falling down on its side; 5, tonic-clonic seizure, falling down on its back, wildly rushing and jumping; 6: death. Scores 4 and above are considered as GSs. The latency to develop GS and the duration of the GS was measured based on the videos. To evaluate the PAX effect on the PTZ induced seizure, a single dose of PAX (0.35 mg/kg, i.p.) or saline control was coinjected with PTZ (40 mg/kg, i.p.).

Drug Treatment for Absence Seizure. To evaluate drug effects on the absence seizure, we only tested the $BK^{DG/DG}$ mice due to their more consistent and higher-frequency spontaneous absence seizures. After 1 h of recording as baseline, a single dose of PAX (0.35 mg/kg, i.p.), ESM (150 mg/kg, i.p.), valproate (200 mg/kg, i.p.), or saline control was injected into the mice.

Open Field Test. The mice were placed in a 45- × 45-cm arena composed of four white Plexiglas walls. They could freely move in the arena for 15 min and their locomotion was continuously monitored by video recording. Locomotor activities were evaluated as the distance traveled per 5 min and the total distance by using a custom MATLAB code. For the PAX treatment experiments, a single dose of PAX (0.35 mg/kg, i.p.) or saline control was injected into the mice 5 min before the test.

Balance Beam Test. Mice were given five training trials on an 80-cm long, 7-mm-diameter small round beam elevated 30 cm above the table, as described

previously (70). A video camera was placed 4 inches away from the starting point, so the hind-paws slip could be easily recorded, whereas the opposite end of the beam entered their home cage with food pellets and bedding materials. The number of foot slips and traversal time were measured as mice traversed the beam in a test trial 24 h after training. For the PAX treatment experiments, a single dose of PAX (0.35 mg/kg, i.p.) or saline control was injected into the mice 5 min before the test.

Accelerating Rotarod. The rotarod treadmills (ENV-577M; Med associates) was used to asset the motor coordination of the mice. Before testing, all mice were trained on a fixed-speed protocol at 4 rpm until they could stay on the rod for 30 s. On the same day as the training session, mice were placed on the rotarod for four 10-min trials with 30-min rest between trials. In each trial, the rotarod accelerated from 4 to 40 rpm at the rate of 1 rpm every 8 s, then remained at 40 rpm until the end of the trial. The time until the mouse fell from the rod was recorded as the latency to fall. The assessments were performed for 4 d. For the PAX treatment experiments, a single dose of PAX (0.35 mg/kg, i.p.) or saline control was injected into the mice 5 min before the test before the daily rotarod test.

Gait Analysis. The forepaws and hind paws of the mice were painted with nontoxic red and blue inks, respectively. After a 2-min habituation trial, each mouse could walk along a narrow, paper-covered runway. The length of each stride was measured. For the PAX treatment experiments, a single dose of PAX (0.35 mg/kg, i.p.) or saline control was injected into the mice 5 min before the test.

Ethanol-Induced Dyskinesia. After habituating in a transparent plastic cage for 10 min, the $BK^{WT/WT}$, $BK^{DG/WT}$, and $BK^{DG/DG}$ mice were injected with diluted ethanol (i.p. 0.5 g/kg body weight, pure ethanol was diluted to 20% [vol/vol] by saline solution 0.9% NaCl). A video camera was placed in front of the cage. The animals were videotaped for 60 min. The onset of a dyskinesia-like attack was signaled by over extension of the hindlimbs, causing an involuntary movement of the body. The number of dyskinesia-like attacks was counted during the 60-min test.

Oxotremorine-Induced Dyskinesia. After habituating in a transparent plastic cage for 10 min, the $BK^{WT/WT}$, $BK^{DG/WT}$, and $BK^{DG/DG}$ mice were injected with oxotremorine methiodide (i.p. 0.01 mg/kg body weight, Sigma-Aldrich, dissolved in saline solution 0.9% NaCl). A video camera was placed in front of the cage. The animals were videotaped for 60 min and motor behavior assessed every 10 min using a previously proposed scale for quantification of abnormal movements and postures (46).

Tail Suspension Test. The mice were suspended by their tails for 30 s. The percentage of animals displaying clasping behavior was calculated through video analysis.

Electrophysiology. For the recording performed in brain slice, acute slice preparations were as described previously (71, 72). Briefly, $BK^{WT/WT}$, $BK^{DG/WT}$, and $BK^{DG/DG}$ mice (from 3 wk to 6 mo) were anesthetized with isoflurane and decapitated. For the recording in different brain regions, the section orientation is different. For the recording in the cortex, 300-μm coronal sections were prepared, and the pyramidal neurons from the layer V/VI of the somatosensory cortex were recorded. For the cerebellar PCs, 250-μm sagittal slices were prepared. The brain slices were cut in ice-cold N-methyl-D-glucamine (NMDG) artificial cerebrospinal fluid (aCSF) containing (in millimolar): 92 NMDG, 2.5 KCl, 1.2 NaH_2PO_4, 30 $NaHCO_3$, 20 HEPES, 25 glucose, 5 sodium ascorbate, 2 thiourea, 3 sodium pyruvate, 10 $MgSO_4{\cdot}7H_2O$, and 0.5 $CaCl_2{\cdot}2H_2O$ (titrated pH to 7.3 to 7.4 using concentrated HCl). The slices were then incubated in HEPES holding solution (in millimolar): 92 NaCl, 2.5 KCl, 1.2 NaH_2PO_4, 25 $NaHCO_3$, 20 HEPES, 25 glucose, 5 sodium ascorbate, 2 thiourea, 3 sodium pyruvate, 2 $MgSO_4{\cdot}7H_2O$, and 2 $CaCl_2{\cdot}2H_2O$ for 60 min at room temperature. After incubation, the slices were transferred to a recording chamber and superfused (3 mL/min) with aCSF at 33 °C (in millimolar): 124 NaCl, 2.5 KCl, 1.2 NaH_2PO_4, 24 $NaHCO_3$, 5 HEPES, 12.5 glucose, 2 $MgSO_4{\cdot}7H_2O$, and 2 $CaCl_2{\cdot}2H_2O$. All solutions used for electrophysiology were equilibrated with 95% O_2/5% CO_2. Whole-cell recordings were performed with a MultiClamp 700B amplifier and sampled at 10 kHz using a Digidata1550A A/D converter. All data acquisition and analyses were performed using the software pClamp 10.7 (Molecular Devices). For AP recording, pipette resistance was 3 to 7 MΩ when filled with an intracellular solution containing the following (in millimolar): 125 K-gluconate, 15 KCl, 10 HEPES, 2 Mg-ATP, 0.3 Na-GTP, 10 disodium phosphocreatine, and 0.2 EGTA, adjusted to pH 7.25 with KOH. After GΩ-seal and membrane breakthrough, the membrane resting potential was monitored for 10 min until it is stabilized before recording of APs. For pharmacological experiments, 10 μM PAX was added to extracellular aCSF. The instant frequency of the AP was analyzed by the build-in function "Threshold Event Detection" from the Clampfit 10.7 (Molecular Devices), and the overall frequency of the AP was calculated by the average of all the instant frequency of the AP events under same current injection condition. AP90% duration was defined by AP duration of 90% repolarization. The fAHP size was measured as the difference between the spike threshold and voltage minimum after the AP. The AP90 and AHP were measured at the first AP of each trace. Input resistance (R_{in}) was calculated from voltage deflections induced by rectangular hyperpolarizing current injections (0 to 100 pA). Membrane time constant (τ_m) was obtained by fitting a single exponential function to these same hyperpolarizing voltage deflections. C_m was calculated by dividing τ_m by R_{in}. AP amplitude was calculated as the voltage difference between AP threshold and AP peak.

Histology. Mice were transcardially perfused with phosphate-buffered saline (PBS) followed by 4% paraformaldehyde. The brain was removed and postfixed in 4% paraformaldehyde overnight at 4 °C and dehydrated in 30% sucrose for 48 h. Sagittal sections (50 μm) containing the cerebellum PCs were collected by using a cryostat (Leica CM1900). The sections were rinsed three times with PBS for 10 min each and blocked with 5% goat serum and 0.3% Triton X-100 for 2 h at room temperature and incubated for overnight at 4 °C with following primary antibodies: anti-calbindin (C9848, 1:1,000, mouse; Sigma-Aldrich). After three rinses with PBS for 10 min, secondary antibodies (A-11032, 1:1,000, conjugated with goat anti-mouse Alexa 594; Thermo Fisher Scientific) were incubated for 2 h at room temperature. Then, the sections were washed three times with PBS for 10 min each and stained with DAPI (1:10,000 of 5 mg/mL; Sigma-Aldrich). Images were acquired using a Zeiss 780 inverted confocal microscope. Representative images were taken from at least three repeats.

Statistics. All the statistical analyses were performed using GraphPad Prism (GraphPad Software). Sample number (*n*) values are indicated in the *Results* and figure legends. All data are presented as the mean ± SEM. Sample sizes were chosen based on standards in the field as well as previous experience with phenotype comparisons. No statistical methods were used to predetermine sample size.

Data Availability. All study data are included in the article and/or supporting information. All the MATLAB codes supporting the present study are available at GitHub (https://github.com/superdongping/PNAS).

ACKNOWLEDGMENTS. We thank Dr. Xuechu Zhen (Soochow University, China) for providing the BK-D434G mice; Dr. Dwight D. Koeberl for his technical assistance with locomotor behavioral tests; and Drs. James O. McNamara, Andrea L. Meredith, William Wetsel, Pengfei Liang, Son Le, Trieu Le, and Zoe Shan for their critical comments on the manuscript. This work was supported by the Duke Institute for Brain Sciences (to M.A.M. and H.Y.) and American Epilepsy Society Post-Doctoral Fellowship 693905 (to P.D.).

Author affiliations: [a]Department of Biochemistry, Duke University Medical Center, Durham, NC 27710; [b]Department of Pediatrics, Duke University Medical Center, Durham, NC 27710; [c]Department of Neurobiology, Duke University Medical Center, Durham, NC 27710; and [d]Department of Biomedical Engineering, Washington University in Saint Louis, Saint Louis, MO 63130

1. C. Contet, S. P. Goulding, D. A. Kuljis, A. L. Barth, BK channels in the central nervous system. *Int. Rev. Neurobiol.* **128**, 281–342 (2016).
2. U. Sausbier *et al.*, Ca^{2+}-activated K^+ channels of the BK-type in the mouse brain. *Histochem. Cell Biol.* **125**, 725–741 (2006).
3. H. G. Knaus *et al.*, Distribution of high-conductance Ca(2+)-activated K^+ channels in rat brain: Targeting to axons and nerve terminals. *J. Neurosci.* **16**, 955–963 (1996).
4. L. Salkoff, A. Butler, G. Ferreira, C. Santi, A. Wei, High-conductance potassium channels of the SLO family. *Nat. Rev. Neurosci.* **7**, 921–931 (2006).
5. H. Berkefeld *et al.*, BKCa-Cav channel complexes mediate rapid and localized Ca^{2+}-activated K^+ signaling. *Science* **314**, 615–620 (2006).
6. R. W. Turner, G. W. Zamponi, T-type channels buddy up. *Pflugers Arch.* **466**, 661–675 (2014).

7. R. Latorre *et al.*, Molecular determinants of BK channel functional diversity and functioning. *Physiol. Rev.* **97**, 39–87 (2017).
8. H. Yang, G. Zhang, J. Cui, BK channels: Multiple sensors, one activation gate. *Front. Physiol.* **6**, 29 (2015).
9. B. Fakler, J. P. Adelman, Control of K(Ca) channels by calcium nano/microdomains. *Neuron* **59**, 873–881 (2008).
10. H. Yang, J. Cui, "BK channels" in *Handbook of Ion Channels*, J. Zheng, C. Matthew, Eds. (CRC Press, 2015), chap. 17.
11. N. Gu, K. Vervaeke, J. F. Storm, BK potassium channels facilitate high-frequency firing and cause early spike frequency adaptation in rat CA1 hippocampal pyramidal cells. *J. Physiol.* **580**, 859–882 (2007).
12. R. Brenner *et al.*, BK channel beta4 subunit reduces dentate gyrus excitability and protects against temporal lobe seizures. *Nat. Neurosci.* **8**, 1752–1759 (2005).
13. W. Du *et al.*, Calcium-sensitive potassium channelopathy in human epilepsy and paroxysmal movement disorder. *Nat. Genet.* **37**, 733–738 (2005).
14. X. Li *et al.*, De novo BK channel variant causes epilepsy by affecting voltage gating but not Ca^{2+} sensitivity. *Eur. J. Hum. Genet.* **26**, 220–229 (2018).
15. G. Yeşil *et al.*, Expanding the phenotype of homozygous *KCNMA1* mutations; Dyskinesia, epilepsy, intellectual disability, cerebellar and corticospinal tract atrophy. *Balkan Med. J.* **35**, 336–339 (2018).
16. B. Tabarki, N. AlMajhad, A. AlHashem, R. Shaheen, F. S. Alkuraya, Homozygous KCNMA1 mutation as a cause of cerebellar atrophy, developmental delay and seizures. *Hum. Genet.* **135**, 1295–1298 (2016).
17. G. Zhang *et al.*, A gain-of-function mutation in KCNMA1 causes dystonia spells controlled with stimulant therapy. *Mov. Disord.* **35**, 1868–1873 (2020).
18. L. Liang *et al.*, De novo loss-of-function KCNMA1 variants are associated with a new multiple malformation syndrome and a broad spectrum of developmental and neurological phenotypes. *Hum. Mol. Genet.* **28**, 2937–2951 (2019).
19. X. Du *et al.*, Loss-of-function BK channel mutation causes impaired mitochondria and progressive cerebellar ataxia. *Proc. Natl. Acad. Sci. U.S.A.* **117**, 6023–6034 (2020).
20. C. Buckley *et al.*, Status dystonicus, oculogyric crisis and paroxysmal dyskinesia in a 25 year-old woman with a novel *KCNMA1* variant, K457E. *Tremor Other Hyperkinet. Mov. (N. Y.)* **10**, 49 (2020).
21. Z. B. Zhang, M. Q. Tian, K. Gao, Y. W. Jiang, Y. Wu, De novo KCNMA1 mutations in children with early-onset paroxysmal dyskinesia and developmental delay. *Mov. Disord.* **30**, 1290–1292 (2015).
22. J. Heim *et al.*, Cataplexy in patients harboring the KCNMA1 p.N999S mutation. *Mov. Disord. Clin. Pract. (Hoboken)* **7**, 861–862 (2020).
23. P. Kratschmer *et al.*, Impaired pre-motor circuit activity and movement in a *Drosophila* model of KCNMA1-linked dyskinesia. *Mov. Disord.* **36**, 1158–1169 (2021).
24. C. S. Bailey, H. J. Moldenhauer, S. M. Park, S. Keros, A. L. Meredith, KCNMA1-linked channelopathy. *J. Gen. Physiol.* **151**, 1173–1189 (2019).
25. H. Wu *et al.*, Phenotype-to-genotype approach reveals head-circumference-associated genes in an autism spectrum disorder cohort. *Clin. Genet.* **97**, 338–346 (2020).
26. P. Y. Deng *et al.*, FMRP regulates neurotransmitter release and synaptic information transmission by modulating action potential duration via BK channels. *Neuron* **77**, 696–711 (2013).
27. A. X. Sun *et al.*, Potassium channel dysfunction in human neuronal models of Angelman syndrome. *Science* **366**, 1486–1492 (2019).
28. J. P. Miller, H. J. Moldenhauer, S. Keros, A. L. Meredith, An emerging spectrum of variants and clinical features in *KCNMA1*-linked channelopathy. *Channels (Austin)* **15**, 447–464 (2021).
29. P. N'Gouemo, Targeting BK (big potassium) channels in epilepsy. *Expert Opin. Ther. Targets* **15**, 1283–1295 (2011).
30. C. S. Bailey, H. J. Moldenhauer, S. M. Park, S. Keros, A. L. Meredith, *KCNMA1*-linked channelopathy. *J. Gen. Physiol.* **151**, 1173–1189 (2019).
31. J. Cui, BK channel gating mechanisms: Progresses toward a better understanding of variants linked neurological diseases. *Front. Physiol.* **12**, 762175 (2021).
32. V. Crunelli *et al.*, Clinical and experimental insight into pathophysiology, comorbidity and therapy of absence seizures. *Brain* **143**, 2341–2368 (2020).
33. J. Yang *et al.*, An epilepsy/dyskinesia-associated mutation enhances BK channel activation by potentiating Ca^{2+} sensing. *Neuron* **66**, 871–883 (2010).
34. B. Wang, B. S. Rothberg, R. Brenner, Mechanism of increased BK channel activation from a channel mutation that causes epilepsy. *J. Gen. Physiol.* **133**, 283–294 (2009).
35. U. S. Lee, J. Cui, β subunit-specific modulations of BK channel function by a mutation associated with epilepsy and dyskinesia. *J. Physiol.* **587**, 1481–1498 (2009).
36. A. Clemente-Perez *et al.*, Distinct thalamic reticular cell types differentially modulate normal and pathological cortical rhythms. *Cell Rep.* **19**, 2130–2142 (2017).
37. K. Sarkisova, G. van Luijtelaar, The WAG/Rij strain: A genetic animal model of absence epilepsy with comorbidity of depression [corrected]. *Prog. Neuropsychopharmacol. Biol. Psychiatry* **35**, 854–876 (2011).
38. D. Liu *et al.*, A common hub for sleep and motor control in the substantia nigra. *Science* **367**, 440–445 (2020).
39. V. Crunelli, N. Leresche, Childhood absence epilepsy: Genes, channels, neurons and networks. *Nat. Rev. Neurosci.* **3**, 371–382 (2002).
40. K. K. Borowicz, B. Piskorska, B. Stępniak, S. J. Czuczwar, Effects of fluoxetine on the anticonvulsant action of valproate and ethosuximide in mouse model of myoclonic convulsions. *Ann. Agric. Environ. Med.* **19**, 487–490 (2012).
41. Y. Zhou, C. J. Lingle, Paxilline inhibits BK channels by an almost exclusively closed-channel block mechanism. *J. Gen. Physiol.* **144**, 415–440 (2014).
42. J. J. Sheehan, B. L. Benedetti, A. L. Barth, Anticonvulsant effects of the BK-channel antagonist paxilline. *Epilepsia* **50**, 711–720 (2009).
43. N. Mehranfard, H. Gholamipour-Badie, F. Motamedi, M. Janahmadi, N. Naderi, The effect of paxilline on early alterations of electrophysiological properties of dentate gyrus granule cells in pilocarpine-treated rats. *Iran. J. Pharm. Res.* **13** (suppl.), 125–132 (2014).
44. S. P. Brooks, S. B. Dunnett, Tests to assess motor phenotype in mice: A user's guide. *Nat. Rev. Neurosci.* **10**, 519–529 (2009).
45. N. E. Mencacci *et al.*, Biallelic variants in TSPOAP1, encoding the active-zone protein RIMBP1, cause autosomal recessive dystonia. *J. Clin. Invest.* **131**, e140625 (2021).
46. A. Pelosi, F. Menardy, D. Popa, J. A. Girault, D. Hervé, Heterozygous Gnal mice are a novel animal model with which to study dystonia pathophysiology. *J. Neurosci.* **37**, 6253–6267 (2017).
47. M. Sausbier *et al.*, Cerebellar ataxia and Purkinje cell dysfunction caused by Ca^{2+}-activated K^+ channel deficiency. *Proc. Natl. Acad. Sci. U.S.A.* **101**, 9474–9478 (2004).
48. X. Chen *et al.*, Disruption of the olivo-cerebellar circuit by Purkinje neuron-specific ablation of BK channels. *Proc. Natl. Acad. Sci. U.S.A.* **107**, 12323–12328 (2010).
49. J. Huguenard, Current controversy: Spikes, bursts, and synchrony in generalized absence epilepsy: Unresolved questions regarding thalamocortical synchrony in absence epilepsy. *Epilepsy Curr.* **19**, 105–111 (2019).
50. G. H. Tan *et al.*, PRRT2 deficiency induces paroxysmal kinesigenic dyskinesia by regulating synaptic transmission in cerebellum. *Cell Res.* **28**, 90–110 (2018).
51. M. M. Shah, Cortical HCN channels: Function, trafficking and plasticity. *J. Physiol.* **592**, 2711–2719 (2014).
52. S. Mi Park *et al.*, BK channel properties correlate with neurobehavioral severity in three KCNMA1-linked channelopathy mouse models. 10.1101/2022.02.15.478992 (16 February 2022).
53. S. K. Kessler, E. McGinnis, A practical guide to treatment of childhood absence epilepsy. *Paediatr. Drugs* **21**, 15–24 (2019).
54. F. T. Zimmerman, B. B. Burgemeister, A new drug for petit mal epilepsy. *Neurology* **8**, 769–775 (1958).
55. M. Z. Gören, F. Onat, Ethosuximide: From bench to bedside. *CNS Drug Rev.* **13**, 224–239 (2007).
56. A. Chapman, P. E. Keane, B. S. Meldrum, J. Simiand, J. C. Vernieres, Mechanism of anticonvulsant action of valproate. *Prog. Neurobiol.* **19**, 315–359 (1982).
57. T. A. Glauser *et al.*; Childhood Absence Epilepsy Study Group, Ethosuximide, valproic acid, and lamotrigine in childhood absence epilepsy. *N. Engl. J. Med.* **362**, 790–799 (2010).
58. M. M. Goldenberg, Overview of drugs used for epilepsy and seizures: Etiology, diagnosis, and treatment. *P T* **35**, 392–415 (2010).
59. M. D. Mark *et al.*, Delayed postnatal loss of P/Q-type calcium channels recapitulates the absence epilepsy, dyskinesia, and ataxia phenotypes of genomic Cacna1a mutations. *J. Neurosci.* **31**, 4311–4326 (2011).
60. M. R. Tanner *et al.*, KCa1.1 inhibition attenuates fibroblast-like synoviocyte invasiveness and ameliorates disease in rat models of rheumatoid arthritis. *Arthritis Rheumatol.* **67**, 96–106 (2015).
61. C. Hisatsune *et al.*, IP3R1 deficiency in the cerebellum/brainstem causes basal ganglia-independent dystonia by triggering tonic Purkinje cell firings in mice. *Front. Neural Circuits* **7**, 156 (2013).
62. R. Fremont, D. P. Calderon, S. Maleki, K. Khodakhah, Abnormal high-frequency burst firing of cerebellar neurons in rapid-onset dystonia-parkinsonism. *J. Neurosci.* **34**, 11723–11732 (2014).
63. Y. Sakai *et al.*, Hyperactivation of mTORC1 disrupts cellular homeostasis in cerebellar Purkinje cells. *Sci. Rep.* **9**, 2799 (2019).
64. M. F. Bastide *et al.*, Pathophysiology of L-dopa-induced motor and non-motor complications in Parkinson's disease. *Prog. Neurobiol.* **132**, 96–168 (2015).
65. J. A. Obeso *et al.*, Pathophysiology of the basal ganglia in Parkinson's disease. *Trends Neurosci.* **23** (10, suppl.), S8–S19 (2000).
66. W. L. Imlach *et al.*, The molecular mechanism of "ryegrass staggers," a neurological disorder of K^+ channels. *J. Pharmacol. Exp. Ther.* **327**, 657–664 (2008).
67. P. Van Hese, J. P. Martens, L. Waterschoot, P. Boon, I. Lemahieu, Automatic detection of spike and wave discharges in the EEG of genetic absence epilepsy rats from Strasbourg. *IEEE Trans. Biomed. Eng.* **56**, 706–717 (2009).
68. T. Shimada, K. Yamagata, Pentylenetetrazole-induced kindling mouse model. *J. Vis. Exp.* **136**, 56573 (2018).
69. R. J. Racine, Modification of seizure activity by electrical stimulation. II. Motor seizure. *Electroencephalogr. Clin. Neurophysiol.* **32**, 281–294 (1972).
70. A. S. Hunanyan *et al.*, Knock-in mouse model of alternating hemiplegia of childhood: Behavioral and electrophysiologic characterization. *Epilepsia* **56**, 82–93 (2015).
71. J. T. Ting *et al.*, Preparation of acute brain slices using an optimized N-methyl-D-glucamine protective recovery method. *J. Vis. Exp.* **132**, e53825 (2018).
72. P. Dong *et al.*, A novel cortico-intrathalamic circuit for flight behavior. *Nat. Neurosci.* **22**, 941–949 (2019).
73. S. Livingston, L. Kajdi, E. M. Bridge, The use of benzedrine and dexedrine sulfate in the treatment of epilepsy. *J. Pediatr.* **32**, 490–494 (1948).
74. C. F. Fletcher *et al.*, Absence epilepsy in tottering mutant mice is associated with calcium channel defects. *Cell* **87**, 607–617 (1996).
75. J. L. Noebels, R. L. Sidman, Inherited epilepsy: Spike-wave and focal motor seizures in the mutant mouse tottering. *Science* **204**, 1334–1336 (1979).
76. A. M. Coenen, W. H. Drinkenburg, M. Inoue, E. L. van Luijtelaar, Genetic models of absence epilepsy, with emphasis on the WAG/Rij strain of rats. *Epilepsy Res.* **12**, 75–86 (1992).
77. I. S. Midzianovskaia, G. D. Kuznetsova, A. M. Coenen, A. M. Spiridonov, E. L. van Luijtelaar, Electrophysiological and pharmacological characteristics of two types of spike-wave discharges in WAG/Rij rats. *Brain Res.* **911**, 62–70 (2001).